Full toroidal imaging of non-axisymmetric plasma material interaction in the National Spherical Torus Experiment divertor[a]

Filippo Scotti,[1,b] A. L. Roquemore,[1] and V. A. Soukhanovskii[2]
[1]*Princeton Plasma Physics Laboratory, Princeton, New Jersey 08543, USA*
[2]*Lawrence Livermore National Laboratory, Livermore, California 94551, USA*

A pair of two dimensional fast cameras with a wide angle view (allowing a full radial and toroidal coverage of the lower divertor) was installed in the National Spherical Torus Experiment in order to monitor non-axisymmetric effects. A custom polar remapping procedure and an absolute photometric calibration enabled the easier visualization and quantitative analysis of non-axisymmetric plasma material interaction (e.g., strike point splitting due to application of 3D fields and effects of toroidally asymmetric plasma facing components). © *2012 American Institute of Physics*. [http://dx.doi.org/10.1063/1.4739510]

I. INTRODUCTION

In magnetic confinement devices, a divertor configuration is employed to concentrate the plasma material interaction away from the core plasma interface. In diverted tokamaks, toroidal axisymmetry for particle and heat fluxes at the divertor plates is usually assumed. However, there are often cases when this assumption is not valid. In the National Spherical Torus Experiment (NSTX), lithium coatings are applied on the lower divertor plasma facing components (PFCs) as a wall conditioning technique by means of two LIThium EvaporatoRs, called LITERs and separated toroidally by 150°.[1] Four toroidal segments of a porous molybdenum surface (separated by an ATJ graphite tile) were installed in the outer divertor region.[2] These molybdenum PFCs with heating capabilities (liquid lithium divertor (LLD)) were designed in order to maintain a liquid lithium surface. The capability of independently heating the LLD segments and the presence of different or unevenly coated PFCs are a clear example of possible non-axisymmetric plasma material interaction. Furthermore, in NSTX, the application of 3D magnetic perturbations was shown to result in the outer strike point splitting in helical lobes of heat and particle fluxes.[3]

In order to study non axisymmetric effects in the NSTX divertor, two fast two dimensional cameras with a wide angle view were installed. In this paper, the setup, calibration, and applications are presented.

II. EXPERIMENTAL SETUP

In order to enable a wide angle view of the lower divertor, two re-entrant view ports (3 in. ø, 1/8 in. thick sapphire window at the end of a 3.5 in. ø, 5 in. long pipe) were developed, located 150° apart on the top of the vacuum vessel on Bay E and Bay J (each bay is separated by 30° toroidally,

A-L). A view of the NSTX lower divertor as imaged by one of the two cameras is shown in Figure 1(a). The typical resolution of 256×208 pixels gives a spatial resolution of ~ 0.8 cm. While two different cameras are used for the two view ports, the same setup (shown in Figure 2) is adopted. In each setup, light is collected by a f = 16 mm C-mount lens (Pentax, F/1.4), which provides the desired wide angle view ($\sim 44°$). The collected light is imaged on a coherent optical fiber bundle (Schott IG-163) 4.57 m in length, which consists of 1000×800 10 μm fibers with a transmittance range of 400–1200 nm. The 4.5 m bundle was chosen in order to keep the cameras in a region with lower magnetic fields and neutron fluxes to avoid damages to the camera electronics. A f = 50 mm C-mount lens (Pentax, F/1.4), installed at the camera end of the light guide, collimates the light rays while a f = 25 mm C-mount lens (Pentax, F/1.4) focuses the image on the camera detector and provides the demagnification needed for the image to fill about 1/16 of the sensor. Between the collimating and the focussing lens, a filter wheel is used to change the narrow three cavity bandpass interference filter (ANDOVER, $\Delta \lambda_{FWHM} \sim 1.5$ nm) through which the plasma is imaged. These include C II (658.5 nm), C III (465.0 nm), C IV (580.1 nm), Li I (670.8 nm), Li II (548.5 nm), and D-α (656.1 nm) filters. Both filter wheels are remotely controlled by a VISUAL BASIC application that allows for the interchange of filters between discharges. As mentioned above, two different cameras are employed. The Phantom v710 has a 1280×800 pixel CMOS sensor and a 25.6×16.0 mm sensor area with a 12 bit dynamic range and a maximum frame rate (at 256×208 pixels) of 100 000 fps. The Phantom v7.3 has a 800×600 pixels CMOS sensor and a 17.6 mm $\times 13.2$ mm sensor area with a 14 bit dynamic range and a maximum frame rate of 60 000 fps (at 224×184 pixels). Each camera is controlled by a Labview VI via a stand alone 1 Gigabit fiber optic link that allows the full transfer of the data within the shot cycle (~ 1–10 GB/discharge/camera) with high stability and reliability.

The wide angle view of the imaging lenses, the use of re-entrant ports, and the small major radius of NSTX allowed the
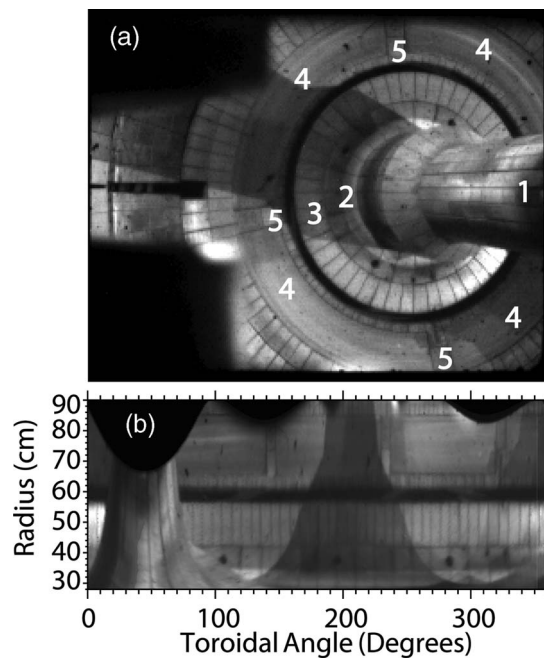

FIG. 1. (a) Bay E lower divertor view: (1) center stack, (2) and (3) 1st and 2nd rows of graphite tiles, respectively, (4) LLD, (5) diagnostic graphite tiles; (b) polar remapping of Bay E view.

FIG. 3. Simulated fresh lithium coatings thickness (top) and measured Li I brightness from the lower divertor (bottom).

imaging of over 50% of the toroidal extent of the divertor on each camera. Remapping the camera data in polar coordinates (radius vs toroidal angle) can be a convenient tool for an easier comparison of radial profiles at different toroidal locations. The intersection of the conic surfaces defined by the collection optics with the divertor plane results in elliptical conic sections. Conic surfaces with increasing subtended angle define ellipses with decreasing elongation. Barrel distortion can lead to a further change in the elongation for structures at different radii. A custom polar remapping routine was developed in order to correct for these effects. In a given field of view, up to five concentric circular divertor structures are fitted to concentric ellipses with different elongations. A polar map is then created where, for every radius, a linear combination of the two closest reference ellipses is used. The camera data are remapped on the polar map and the toroidal angle is linearized to correct for lens distortion. Images of the lower divertor were routinely taken and used to create the polar map as
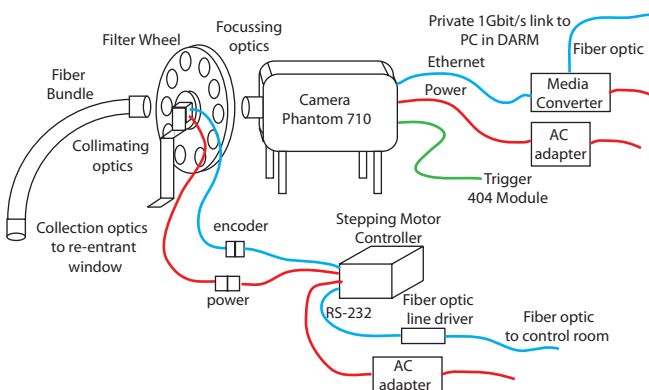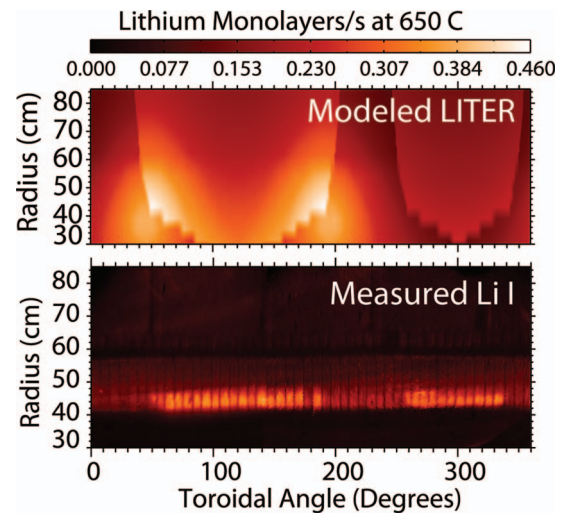
shown in Figure 1(b). Combining the two views, full toroidal imaging of the lower divertor is possible.

In order to quantitatively analyze 2D data, an absolute calibration is performed for the two cameras over the entire field of view. The calibration is done before and after the experimental run to correct for transmittance losses due to fiber degradation and window coatings and it is carried out by means of a high reflectance lambertian target with uniform illumination (whiteplate) and an integrating sphere. The relative sensitivity of the system is calibrated using the whiteplate. The whiteplate is positioned *in situ* in three different locations and the three calibrations are combined to obtain the 2D relative sensitivity, which is then absolutely scaled using the luminance of the integrating sphere. The absolute brightness of each spectral line measured during experiments can then be directly related to influxes of specific ionic species using the S/XB (inverse photon efficiency) method.[4]

FIG. 2. Schematic of camera setup.

III. APPLICATIONS

A. Toroidal asymmetry in plasma facing components

Full toroidal imaging enabled the analysis of how recycling and impurity influxes vary on different or differently coated PFCs and on PFCs at different temperatures. Simulations[5] show that the lithium evaporation geometry in NSTX can lead to a toroidal variation in the coating thickness up to a factor of 3. Toroidal asymmetries in lithium influxes are generally observed and are enhanced during transient divertor heat loads. The transient heat load causes differential heating of coatings with different thickness and a consequently different lithium sputtering response.[6] In Figure 3 (top), the simulated lithium toroidal distribution is shown. Areas with heavier lithium deposition, as well as areas shadowed by the center stack, can be seen. In Figure 3 (bottom), a full polar plot of divertor Li I brightness is shown, obtained by combining views from both Bay E and Bay J after a Type I edge localized mode (ELM). The two regions in which the LITERs are shadowed by the center stack result
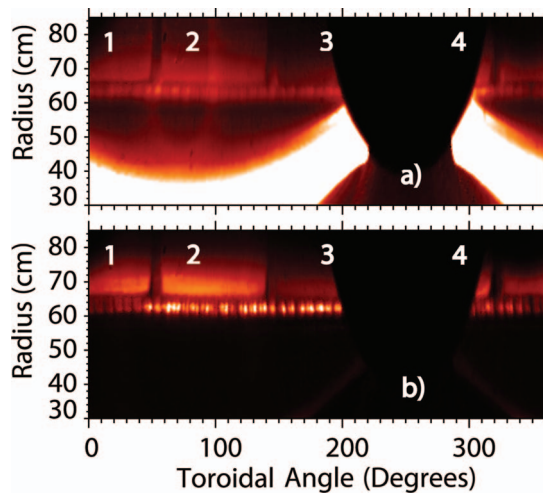
FIG. 4. (a) D-α and (b) Li I emission with heated LLD.

in a lower lithium influx and closely match the simulated distribution.

The response of differently heated PFCs was investigated by externally heating three LLD segments at 220 °C (above the lithium melting point, 180 °C) while the last one was below 180 °C. In these discharges, the outer strike point (OSP) was controlled at R = 63 cm, inboard of the LLD. In Figure 4, the divertor region is imaged through D-α (top) and Li I (bottom) filters. Higher D-α emission can be seen on the warm LLD plates (1, 2, 4 in Figure 4), while the cold LLD segment (3 in Figure 4) is comparable to the nearby graphite tiles. Assuming toroidal symmetry in incident ion fluxes, this indicates increased recycling on the warm LLD plates. Heated LLD segments also clearly show enhanced neutral lithium influxes (up to 2×), as a result of the temperature dependence of lithium sputtering yield.[6]

B. Toroidal asymmetries in plasma surface interaction

The full toroidal imaging allowed the study of the patterns of strike point splitting as a result of the different toroidal spectrum of perturbing 3D fields. For this purpose, Li I imaging was the most effective, thanks to the routine use of lithium conditioning and to the low ionization potential of lithium (∼5 eV) that results in emission localized at the PFCs surface. In NSTX, 3D magnetic perturbations produced by a set of six midplane coils are used for error field correction, resistive wall mode control, and ELM triggering. In Figures 5(a) and 5(b), respectively, an unperturbed toroidally symmetric OSP and an OSP perturbed by the application of $n = 3$ fields are shown. One can notice the spiral structure of particle flux lobes separated toroidally by 120°. Toroidally asymmetric plasma surface interactions can also occur during ELMs as shown in Figure 5(c), where the Li I filter is used to image particle fluxes to the PFCs during a Type V ELM. Toroidally asymmetric auxiliary heating deposition in the plasma edge can result in the non-axisymmetric deposi-
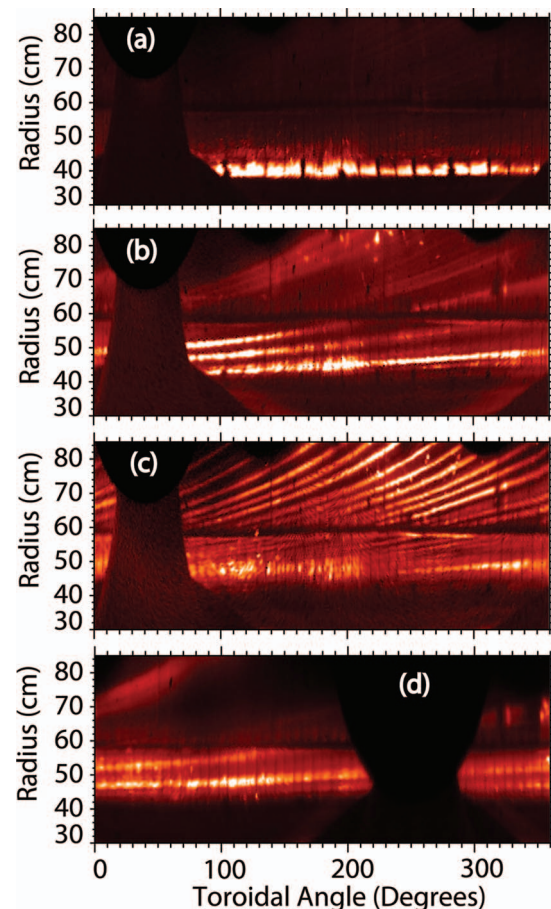

FIG. 5. Measured Li I brightness for (a) unperturbed OSP, (b) OSP splitting with application of $n = 3$ fields, (c) Type V ELM, (d) RF divertor "hot" zone.

tion of divertor heat and particles fluxes. In NSTX, radio frequency (RF) heating by high harmonic fast waves results in a significant fraction of the injected power being coupled to the edge/scrape-off layer plasma and propagating directly to the divertor region, leading to non axisymmetric helical structures with higher particle loads (RF "hot" divertor zone).[7] In Figure 5(d), the spiral structure due to RF heating is shown as imaged by the Li I filter.

ACKNOWLEDGMENTS

[1]M. G. Bell *et al.*, Plasma Phys. Controlled Fusion **51**(12), 124054 (2009).
[2]H. W. Kugel *et al.*, J. Nucl. Mater. **415**, S400–S404 (2011).
[3]J.-W. Ahn *et al.*, Nucl. Fusion **50**(4), 045010 (2010).
[4]K. H. Behringer, J. Nucl. Mater. **145–147**, 145–153 (1987).
[5]L. E. Zakharov, private communication (2011).
[6]J. P. Allain *et al.*, Phys. Rev. B **76**, 205434 (2007).
[7]R. Perkins *et al.*, Phys. Rev. Lett. **109**, 045001 (2012).